8.2 DEVELOPMENT OF ALGORITHMS TO RETRIEVE AEROSOL OPTICAL PROPERTIES FROM DUAL WAVELENGTH POLARIZATION LIDAR AND APPLICATION TO THE LIDAR DATA MEASURED OVER THE TROPICAL PACIFIC OCEAN

Tomoaki Nishizawa*,
Meteorological Research Institute / the Japan Society for the Promotion of Science, Tsukuba, Japan
Hajime Okamto,
Center for Atmospheric and Oceanic Studies, Tohoku University, Sendai, Japan
Toshihiko Takemura,
Research Institute for applied mechanics, Kyusyu University, kasuga, Japan
Nobuo Sugimoto, Ichiro Matsui, and Atsushi Shimizu
National Institute for Environmental Studies, Tsukuba, Japan

1. INTRODUCTION

Grasping temporal and spatial variation of optical and microphysical properties of aerosols is inevitable in order to study the earth's climate. The ship-borne measurement with the research vessel MIRAI of JAMSTEC (Japanese Maritime Science and Technology Center) was conducted on the coast of Indonesia and Philippine islands over the tropical Pacific Ocean from September 21 to December 17, 2001. One of the main features of the ship-borne measurement cruise is that two active instruments, i.e., a dual wavelength polarized Mie-scattering lidar of NIES (National Institute for Environmental Studies) and a 95-GHz cloud profiling radar of NICT (National Institute of Information and Communications Technology) were installed. The analysis of the lidar and radar data can provide information about the temporal and spatial distribution of aerosols and clouds over the ocean, and further is helpful for the validation with products from such numerical models as aerosol transport models and cloud-resolving models.

We developed two types of algorithm: forward and backward. The algorithms can retrieve the extinction coefficients at a wavelength of λ = 532 nm of two types of aerosol component, i.e., water-soluble (σ_{WS}) and sea-salt (σ_{SS}) or water-soluble and dust (σ_{DS}), at a given layer, using information from three-channel lidar measurements, i.e., co-polarization and cross-polarization components at λ = 532 nm and total component (co-polarization + cross-polarization) at λ = 1064 nm. The algorithms are designed to analyze the data measured with the NIES lidar installed on the vessel MIRAI, however, it should be noted that they can be applied to the data measured over ocean with the similar lidar to the NIES one, e.g., the lidar installed on the CALIPSO satellite of NASA. We also applied the two algorithms to the lidar data measured over the tropical Pacific Ocean during the MIRAI cruise.

*Corresponding author address: Tomoaki Nishizawa, Meteorological Research Institute / the Japan Society for the Promotion of Science, Tsukuba, 305-0052, Japan; e-mail: nisizawa@mri-jma.go.jp

2. OBSERVED DATA

Fig. 1 shows the shiptrack of the MIRAI cruise. The lidar data were recorded up to 20 km with 6 m resolution. The signals were averaged every 10 s corresponding to 100 shots. The details about the system of the NIES lidar are described in *Sugimoto et al.* [2000]. In this study, we define the following parameters as the measured data,

$$P_{obs,\lambda}(Z) = \frac{Z^2(P_{\perp,\lambda}(Z) + P_{\parallel,\lambda}(Z))}{\delta Z}, \quad (1)$$

$$\beta_{obs,\lambda}(Z) = \frac{P_{obs,\lambda}(Z)}{C_\lambda}, \quad (2)$$

$$\delta_{obs,\lambda}(Z) = \frac{P_{\perp,\lambda}(Z)}{P_{\parallel,\lambda}(Z)}, \quad (3)$$

where Z is an altitude, $P_\perp$ and $P_\parallel$ are co-polarization and cross-polarization components of the lidar signals, respectively, δZ is a vertical resolution, C is a calibration constant of lidar, and δ_{obs} is a total depolarization ratio. Hereafter, we refer to P_{obs} and β_{obs} as lidar receiving signal strength and attenuated backscattering coefficient, respectively. The spectral ratio of the calibration constant (i.e., C_{532} / C_{1064}) was obtained on the basis of the method of *Sugimoto et al.* [2001].

We used the data measured with the NICT radar in order to remove data contaminated with clouds or drizzle; the cloud mask scheme used in this study is described in section 4. The technical specifications about the NICT radar can be found in *Horie et al.*

[2000]. The radar data were recorded up to 20 km with 82.5 m resolution. The return-signal (P_r) was averaged every 10 s corresponding to about 80,000 shots. Hereafter, we represent the measured data with the following parameter: $dBP_r = 10 \log_{10} P_r$.

We averaged the lidar data every 82.5m in the vertical direction, and further averaged the lidar and radar data every minute. Consequently, we used the lidar and radar data with the temporal and vertical resolution of 82.5m and 1 minuete, respectively, in the analysis. The application of the algorithms to the lidar data is limited to the layers from 0.2 km to 2.5 km owing to the following restrictions: the signal to noise ratio (*SN*-ratio) of the lidar signals is generally worse in the upper layer, in addition, the lidar signals have a blind region near the lidar due to the insufficient overlapping of the laser beam and the field of view of the receiving telescope.

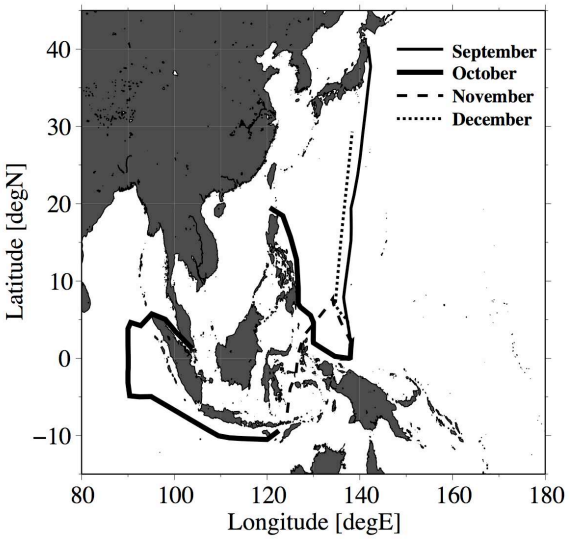

Fig. 1 Shiptrack of the MIRAI cruise

3. ALGORITHMS

The advantages of our algorithms are that they can retrieve the vertical profiles of each aerosol component, and also the vertical profiles of microphysical and optical properties of aerosols such as lidar ratio (i.e., extinction-to-backscattering ratio) and number concentration, distinct from the widely used Fernald's method [*Fernald,* 1984]. The advantage of the forward-type algoritm is that it can retrieve the aerosol properties under a layer of clouds as well as clear-sky condition; this is also an advantage of our algorithms and it is expected that this algorithm can provide knowledge related to aerosol-cloud interaction around cloud bottom layers. It needs the calibrated signals, i.e., attenuated backscattering coefficient. The backward-type algorithm can estimate the calibration constant of lidar as well as the vertical profiles of aerosol properties, however, its application should be limited to the data under clear-sky condition since the data over clouds are contaminated with their strong attenuation and thus it is not possible to calibrate the signals. The characteristic feature of our analysis of aerosols are the combinational use of both algorithms, i.e., the backward-type algorithm is first applied to the lidar data measured under clear-sky condition in order to calibrate the lidar signals as well as retrieve the vertical profiles of aerosols, and then the forward-type algorithm is used to retrieve the aerosol properties under a layer of clouds. The details of the algorithms can be found in *Nishizawa et al.* [2006]. In the following, we only provide the brief description for the algorithms.

(a) *Assumptions of the Algorithms*

The following assumptions have been made in both the algorithms: (1) the volume size distribution of aerosols is assumed to be bimodal, with peaks of lognormal shape. (2) Two types of aerosol model are assumed: the sea-salt and dust models. The sea-salt model consists of two aerosol components: water-soluble aerosols with mode-radius in the fine-mode region and sea-salt aerosols with mode-radius in the coarse-mode region. The dust model also consists of two aerosol components: water-soluble aerosols and dust aerosols with mode-radius in the coarse-mode region. (3) The microphysical and optical properties are assumed for water-soluble, sea-salt and dust particles based on *Hess et al.* [1998] and *Smirnov et al.* [2002] (Table 1). (4) We assume a scale height value of 1.3 km for the vertical profile of the aerosol extinction coefficient under the lowest layer to correct the attenuation of lidar signals.

Properties	Water-soluble	Sea-salt	Dust
r_m	0.13	3.0	3.0
s_d	1.6	2.1	2.2
m	$1.41 - 2\times10^{-3}i$	$1.36 - 3\times10^{-9}i$	$1.53 - 6\times10^{-3}i$
S	55	20	22

Table 1. Optical and microphysical properties assumed in the algorithms. The r_m, s_d, m and S are mode-radius and standard deviation of the size distribution, complex refractive index and lidar ratio, respectively. The values of m and S are at λ = 532 nm. The units of r_m and S are μm and sr, respectively.

(b) *Forward-type Algorithm*

The forward-type algorithm uses the β_{obs} at λ = 532 and 1064 nm and δ_{obs} at λ = 532 nm. It retrieves the vertical profiles of aerosols sequentially from the lowest layer to the highest layer, by repeating the following steps at each layer: (1) retrieving the extinction coefficients of the two aerosol components for each model, i.e., the sea-salt and dust models, that can simulate the β_{obs} at the two wavelengths, (2) determining the model by using the δ_{obs}, and (3) estimating the aerosol optical thickness from the retrieved σ_{WS} and σ_{SS} or σ_{WS} and σ_{DS} in order to correct the attenuation of the β_{obs}. In step 2, we first compute the depolarization ratio of aerosols themselves (δ_a) for each model using the δ_{obs} and the backscattering coefficient of aerosols retrieved for each model. We then determine the model using the following criteria: adopting the sea-salt model / dust model when both the δ_a-values computed for the sea-salt and dust models are smaller / larger than 0.1. There might be cases that the δ_a-values do not match the conditions, e.g., δ_a-values for sea-salt and dust models are larger and smaller than 0.1, respectively. In such cases, the layer is categorized as 'Unknown model' and their optical properties such as extinction coefficient and number concentration for total aerosols are estimated from the σ_{WS} and σ_{DS} obtained using the dust model.

(c) *Backward-type Algorithm*

The backward-type algorithm uses the P_{obs} at λ = 532 and 1064 nm and δ_{obs} at λ = 532 nm. It should be noted that the spectral ratio of P_{obs} (i.e., $P_{obs,\ 532}$ / $P_{obs,1064}$) has to be calibrated in advance. The algorithm retrieves the calibration constant of the lidar and the vertical profiles of aerosols, involving the following steps: (1) setting an appropriate value of extinction coefficient at λ = 532 nm for total aerosols at the highest layer ($\sigma_{a,h}$), (2) retrieving the vertical profiles of aerosols sequentially from the highest layer to the lowest layer, repeating the similar steps as the forward one takes, and (3) computing the values of C at λ = 532 and 1064 nm. In step 2, the extinction and backscattering coefficient of total aerosols at the highest layer are needed to simulate P_{obs} at each layer. We compute those from the value of $\sigma_{a,h}$ using the optical properties of dust particles assumed in the algorithm. We repeat the above steps from (1) to (3) changing the value of $\sigma_{a,h}$, and find solution to match the measured C_{532} / C_{1064}.

(d) *Validation of the Algorithms*

We validated the algorithms using the other MIRAI cruise data; the cruise was carried out over the Pacific Ocean near the Japan island during two weeks in May 2001. In the cruise, the NIES lidar, NICT radar and also sky radiometer (Prede Co. Ltd., POM-01 MKII) were installed on the MIRAI vessel. Then, we compared the optical thickness for total aerosols at λ = 500 nm retrieved by the backward and forward algorithms from the lidar data with those retrieved from the sky radiometer measurements. It turned out to be good agreement between the lidar and sky radiometer measurements: the differences were 2% and 10% in relative error for the backward and forward algorithms, respectively.

4. APPLICATION OF THE ALGORITHMS TO THE MIRAI CRUISE DATA

First of all, we applied the backward-type algorithm to the lidar data without clouds to obtain the calibration constant of the lidar. In order to extract the C-values retrieved from the data under clear-sky condition, we used the following criterion: the dBP_r is smaller than noise level plus 0.5 dB and the retrieved value of backscattering coefficient of total aerosols at λ = 532 nm is smaller than 0.01 km^{-1} in all the layer. After that, the value of C at each time during the whole observation period was linearly interpolated from the C-values for the clear-sky condition, and thus the β_{obs} were obtained (Fig. 2). Next, we removed the data contaminated by clouds and drizzle using the β_{obs} at λ = 1064 nm and the dBP_r. When the lidar or radar data at a given layer fulfill one of the following three criteria, we consider that the layer consists of clouds or drizzle: (1) the dBP_r is larger than noise plus 0.5 dB, (2) the β_{obs} is larger than 0.01 $km^{-1}sr^{-1}$, and (3) the β_{obs} is larger than 0.003 $km^{-1}sr^{-1}$ and the slope of β_{obs} against altitude, i.e., $\delta\beta_{obs}$ / δZ, is larger than 0.025 $km^{-2}sr^{-1}$. The threshold values of the criteria are empirically determined. The data for the upper layer than clouds or drizzle are removed: the data are affected by the strong attenuation due to clouds or precipitation. From the application of the cloud mask scheme to the lidar and radar data, it turned out that the occurrence of clouds and precipitation below the altitude of 2.5 km during the whole observation period was 45 %. Finally, we applied the forward-type algorithm and also the backward-type algorithm to the lidar data after removing clouds and drizzle. Note that in the following results, the optical properties of aerosols for the clear-sky and cloudy condition are basically retrieved by the backward and forward algorithms, respectively. There are some

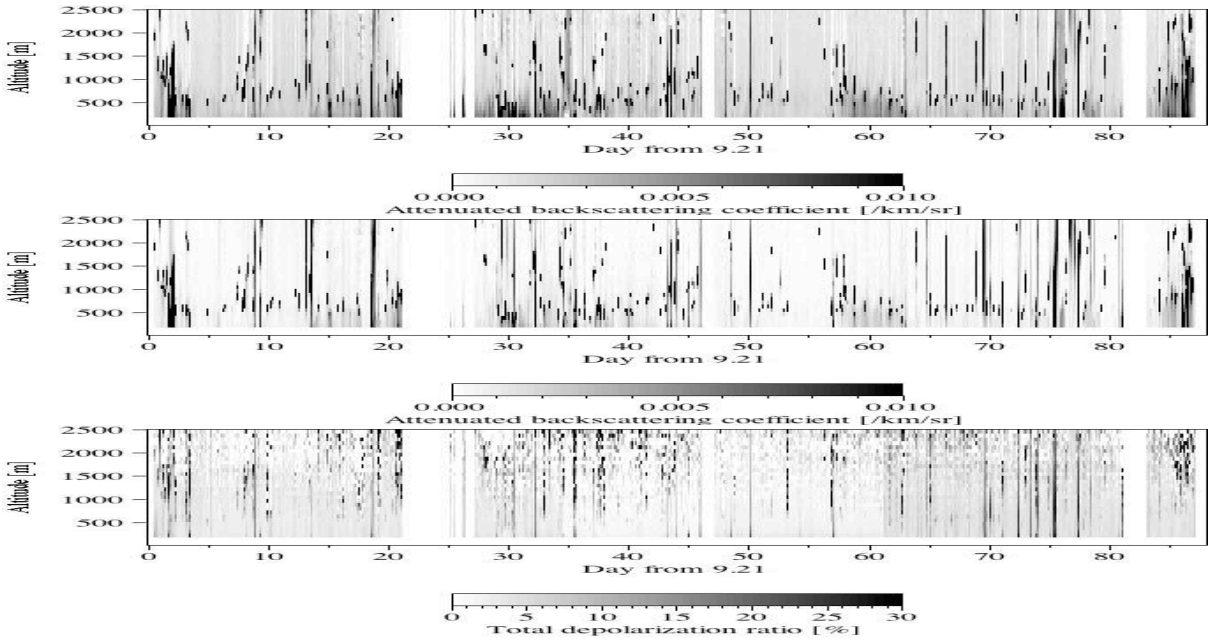

Fig. 2 Time-height cross-section of β_{obs} at λ = 532 nm (upper figure) and 1064 nm (middle figure) and δ_{obs} at λ = 532 nm (lower figure) measured during the whole observation period of the MIRAI cruise.

cases that the backward-type algorithm cannot retrieve the aerosol optical properties although clouds or rain are not found; this is mainly because the *SN*-ratio at a layer where the estimation starts is low and also the aerosol model assumed for the highest layer in the algorithm (see section 3) is inadequate. Then, we show the aerosol optical properties retrieved by the forward-type algorithm.

Fig. 3 shows the extinction coefficient at λ = 532 nm for water-soluble σ_{WS}, sea-salt σ_{SS}, dust σ_{DS} and total aerosols (σ_T) estimated for the whole observation period. Most of water-soluble and sea-salt particles are present below 1 km. Dust particles are hardly found in the whole observation period, and thus the extinction coefficient of total aerosols σ_T are mainly affected by those of water-soluble and sea-salt. The

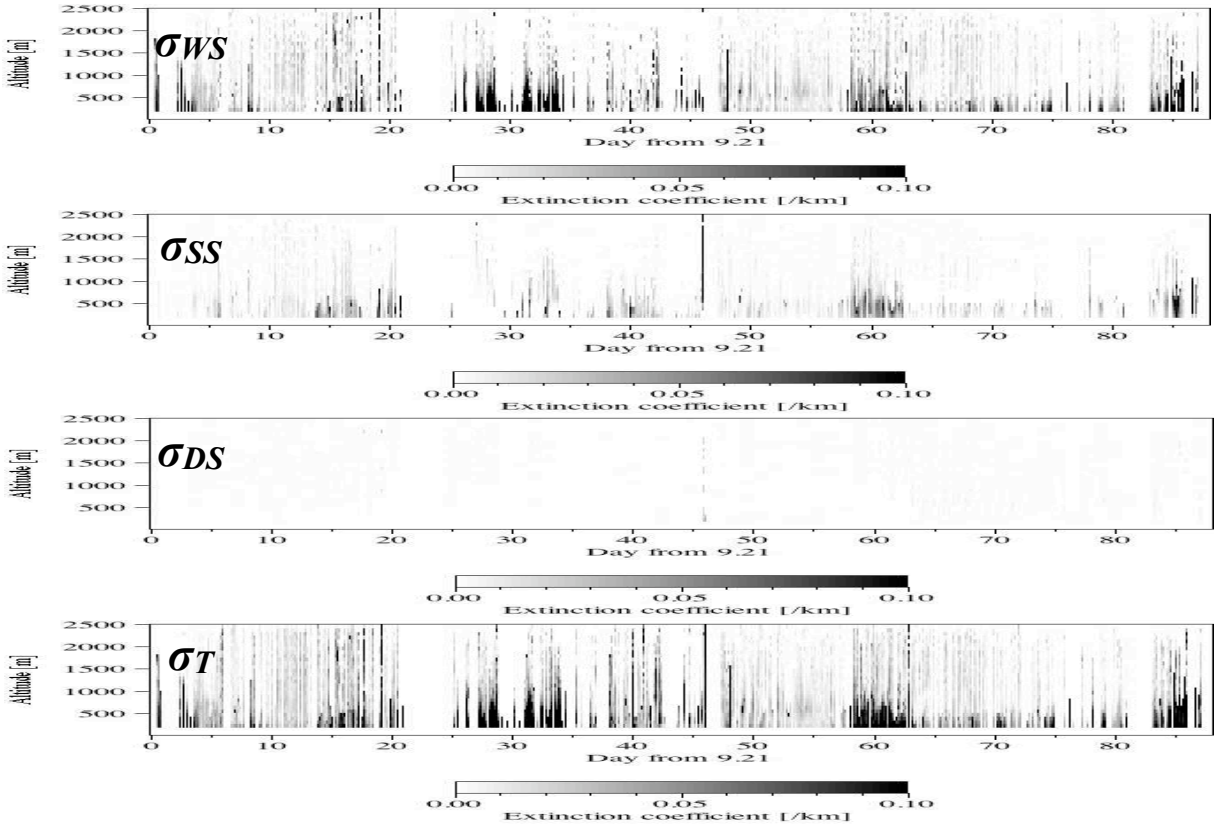

Fig. 3 Time-height cross-section of σ_{WS}, σ_{SS}, σ_{DS} and σ_T for the whole observation period.

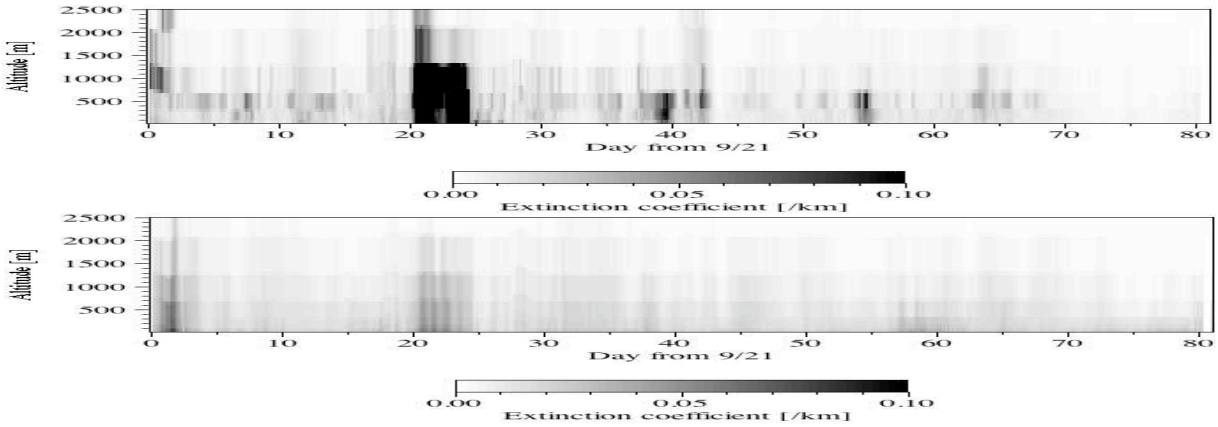

Fig. 4 Time-height cross-section of extinction coefficient at λ = 532 nm for sulfate (upper figure) and sea-salt (lower figure) particles simulated by the SPRINTARS from 21 September to 10 December during the observation period of the MIRAI cruise.

figure also shows that the values of σ_{WS} and σ_{SS} are extremely variable in temporal, e.g., the σ_{WS} are relatively larger around 30th, 60th and 85th day from 21st September than the other days, and the σ_{SS} are relatively large around 15th, 40th, 60th and 85th day from 21st September. It should be noted that the variation of σ_{WS} and σ_{SS} are due to not only temporal variation and also horizontal distribution.

The simulation by the global aerosol transport model, SPRINTARS (Spectral Radiation-Transport Model for Aerosols Species) developed by *Takemura et al.* [2005], were carried out for the observation period of the MIRAI cruise (Fig. 4). We then compare the vertical and temporal distribution of extinction coefficient for sulfate, sea-salt and dust particles simulated by the SPRINTARS with those retrieved from the lidar measurements. In this study, we consider that the sulfate simulated by the SPRINTARS and the water-soluble retrieved from the lidar measurements are similar types of aerosols. The horizontal and temporal resolution of the SPRINTARS's simulation are about 100 km and 40 minutes. The 20 layers from the surface to the altitude of about 33 km are considered in the simulation; the data is interpolated to match the vertical resolution with that of the lidar (i.e., δZ = 82.5m). The results of the simulation by the SPRINTARS show that most of water-soluble and sea-salt particles concentrate below 1 km, and few dust particles are found for the whole observation period; these results are consistent with those retrieved from the lidar measurements. The temporal distribution of sea-salt particles simulated by the SPRINTARS roughly match with that retrieved from the lidar measurements, e.g., the values of σ_{SS} simulated by the SPRINTARS are relatively larger around 60th day from 21st September than the other days. On the other hand, the distribution for water-soluble particles are not in agreement between the SPRINTARS and lidar.

We further investigated the horizontal distribution of aerosols during the observation period. We show the optical thickness for total aerosols retrieved for the whole observation period in Fig. 5. The figure shows that the optical thickness are relatively larger in the region from the Japan island to the island of New Guinea and in the western region off the Sumatra island than the other regions. We also shows the

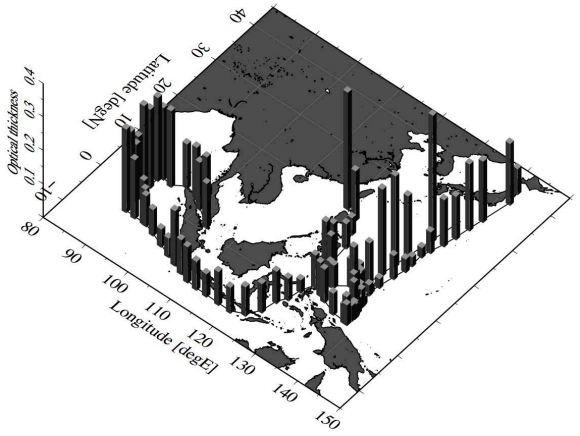

Fig. 5 Spatial distribution of the optical thickness at λ = 532 nm for total aerosols during the whole observation period.

latitudinal distribution of the aerosol optical thickness in the region between 0 and 40 degN and between 130 and 140 degE, which corresponds to the region from the Japan island to the island of New Guinea, and also the longitudinal distribution in the region between 90 and 140 degE and between -10 and 10 degN, which corresponds to the region from the western part off the Sumatra to the island of the New Guinea, in Fig. 6, where we averaged the retrieved optical thickness every 0.5 degree. The optical thickness for total aerosols generally becomes larger as the

latitude increases or the longitude decreases; the water-soluble particles are the major contributor to the the total optical thickness of aerosols. Since the optical thickness reported from sunphotometry measurements over the open sea in the Pacific region are generally smaller than 0.1 [e.g., see *Smirnov et al.,* 2002], it is suggested that the results imply advection of aerosols originated from the lands such as Indonesia, Philippine and Japan islands.

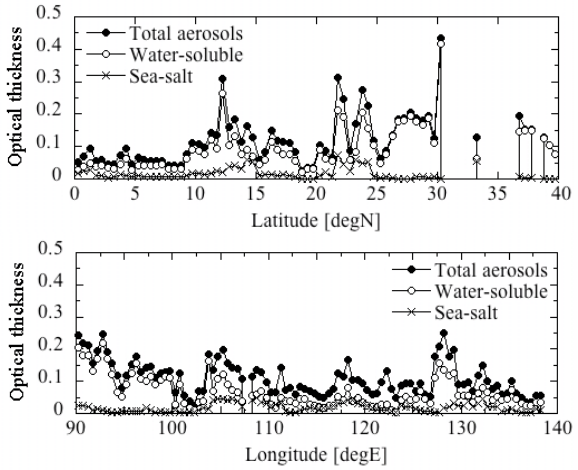

Fig. 6 Latitudinal (upper figure) and longitudinal (lower figure) distribution of the optical thickness at λ = 532 nm for each aerosol component.

5. SUMMARY

We have developed two types of algorithms, i.e., forward and backward, to retrieve the extinction coefficient at a wavelength of λ = 532 nm for two types of aerosols , i.e., water-soluble and sea-salt or water-soluble and dust, at each layer from the dual wavelength polarized lidar measurements. Distinct from the algorithms developed to date, our algorithms can determine aerosol types and retrieve the vertical profiles of the lidar ratio and number concentration.

We applied the algorithms to the data measured with the dual-wavelength polarized lidar of NIES installed on the vessel MIRAI over the tropical Pacific Ocean. The highlighted results are as follows:

(1) Major components are water soluble and sea-salt and only a few dust particles were found in the whole observation period. Most of water-soluble and sea-salt particles exist below 1 km.

(2) The overall pattern of the vertical and temporal distribution for sulfate, sea-salt and dust particles simulated by the SPRINTARS roughly in good agreement with those retrieved from the lidar measurements, except for the temporal distribution of sulfate particles.

(3) The optical thickness for total aerosols increases as the latitude becomes higher or the longitude becomes lower. The distribution of the optical thickness for total aerosols is mainly affected by the water-soluble particles.

We are planning to conduct quantitative comparison between the lidar and SPRINTARS, e.g., direct comparing the values of the extinction coefficient for each aerosol type. We will also apply the algorithms to the lidar data measured in the other MIRAI cruises, e.g., in the region between the Japan island and the island of New Guinea over the tropical Pacific Ocean in 2004. Further, we will apply the algorithms to the CALIPSO lidar data measured over the sea.

Acknowledgements

We are grateful to Dr. K. Yoneyama at JAMSTEC for conducting the atmospheric observation mission on the Research Vessel Mirai. We also thank Dr. H. Kumagai of NICT. This work was partly supported by the Ministry of Education, Culture, Sports, Science, and Technology through a Grant-in-Aid for Scientific Research (No. 14702014) and a Grant-in-Aid for JSPS Fellows (No. 16·2254), by Core Research for Evolutional Science and Technology (CREST) of the Japan Science and Technology Agency, and by the Global Environment Research Fund.

References

Fernald, F. G., 1984: Analysis of atmospheric lidar observations: some comments, *Appl. Opt.*, **23**, 652-653.

Hess, M., P. Koepke, and I. Schult, 1998: Optical properties of aerosols and clouds: The software package OPAC, *Bull. Amer. Meteor. Soc.*, **79**, 831-844.

Horie, H., T. Iguchi, H. Hanado, H. Kuroiwa, H. Okamoto and H. Kumagai, 2000: Development of a 95-GHz Airborne Cloud Profiling Radar (SPIDER): Technical aspects, *IEICE Trans. Commun.,* **E83-B(No. 9)**, 2010-2020.

Nishizawa, T., H. Okamoto, N. Sugimoto, I. Matsui, A. Shimizu and K. Aoki, 2006: An algorithm that retrieves aerosol properties from dual-wavelength polarization lidar measurements, *Submitted to J. Geophys. Res.*.

Smirnov, A., B. N. Holben, Y. J. Kaufman, O. Dubovik, T. F. Eck, I. Slutsker, C. Pietras, and R. N. Halthore, 2002: Optical properties of atmospheric aerosol in maritime environments, *J. Atmos. Sci.* **59**, 501-523

Sugimoto, N., I. Matsui, Z. Liu, A. Shimizu, K. Asai, K. Yoneyama, and M. Katsumata, 2001: Latitudinal distribution of aerosols and clouds in the western Pacific observed with a lidar on board the research vessel Mirai, *Geophys. Res. Lett.,* **28**, 4187-4190.

Sugimoto, N., I. Matsui, Z. Liu, A. Shimizu, I. Tamamushi

and K. Asai, 2000: Observation of aerosols and clouds using a two-wavelength polarization lidar during the Nauru99 experiment, *Journal of The Marine Meteorology Society, UMI TO SORA (SEA AND SKY),* **76**, 90-95.

Takemura, T., T. Nozawa, S. Emori, T. Y. Nakajima, and T. Nakajima, 2005: Simulation of climate response to aerosol direct and indirect effects with aerosol transport-radiation model, *J. Geophys. Res.,* **110**, D02202, doi:10.1029/2004JD005029.